6ICEGE
6th International Conference on Earthquake Geotechnical Engineering
1-4 November 2015
Christchurch, New Zealand

Deformation Mechanisms Under Shallow Foundations During Earthquake-Induced Liquefaction

O. Adamidis[1], G.S.P. Madabhushi[2]

ABSTRACT

Buildings with shallow foundations suffered significant liquefaction-related damage during the recent 2010-2011 series of earthquakes in Christchurch, New Zealand. The way that deformation mechanisms develop under such structures in the event of liquefaction is not well defined. In an effort to shed light on this problem, three dynamic centrifuge tests are presented in this paper. The main parameter investigated is the ratio of the width of the structure's foundation (B) over the depth of the underlying liquefiable layer (D_L). As this parameter (B/D_L) changes, the prevailing mechanisms are presented in a novel way, using displacement vector fields. For smaller values of B/D_L, an extended mechanism is mobilised. The structure moves downwards along with a zone of increased effective stress underneath it, while the surrounding soil is displaced outwards. For larger values of B/D_L, displacements are more localised and are predominantly stemming from cyclic loading imposed due to soil-structure interaction.

Introduction

During the 2010-2011 series of seismic events in Christchurch, New Zealand, earthquake-induced liquefaction was one of the main causes of damage to the built environment (Cubrinovski et al., 2011). In particular, buildings with shallow foundations suffered severely. These buildings, despite being the most common, are not sufficiently protected, as showcased not only by the Christchurch earthquakes but also by other recent events in Turkey (Bray et al., 2004), Chile (Bertalot et al., 2013), and Japan (Yasuda et al., 2012).

The evaluation of settlement is the most sought after aspect of the seismic response of shallow foundations. Yet, it remains elusive. The state-of-the-practice relies on methodologies aimed at predicting one-dimensional, post-liquefaction, free-field settlement (e.g. Tokimatsu and Seed, 1987). However, this approach is wanting.

Free-field methods only account for sedimentation and consolidation. These are volumetric deformation mechanisms affecting the whole liquefiable layer. In reality, several additional mechanisms of a localised nature can contribute to settlement. Dashti et al. (2010) attributed previously unaccounted for volumetric strains to localised partial drainage and diminishing effective stresses. They also stressed the importance of deviatoric strains, due to partial bearing failure or ratcheting of the structure.

[1]PhD Candidate, Department of Engineering, University of Cambridge, Cambridge, UK, oa245@cam.ac.uk
[2]Professor of Civil Engineering, Department of Engineering, University of Cambridge, Cambridge, UK, mspg1@cam.ac.uk

Despite the conceptual identification of settlement-generating mechanisms, their case-specific significance remains unclear. Their contribution to settlement depends on a broad spectrum of parameters related to the liquefiable layer, the structure, and the seismic motion in question (Dashti et al., 2010). Of all possible parameters, it is the depth of the liquefiable layer (D_L) that has come to dominate analyses over the years. Yoshimi and Tokimatsu (1977) introduced the normalisation of both the width (B) of a structure and its expected settlement (S) with the depth of the liquefiable layer, and presented an empirical graph that correlates the two based on the settlement of buildings during the 1964 Niigata earthquake. This graph was later enriched with centrifuge test results (Liu and Dobry, 1997). However, its validity for thin layers (large values of B/D_L) was recently challenged both using centrifuge experiments and real earthquake case-histories (Dashti et al., 2010, Bertalot et al., 2013). The main issue seems to be an inherent bias in favour of volumetric mechanisms affecting the whole layer. In reality, these mechanisms could be of limited significance, especially for thinner layers.

At the core of the problems arising from using B/D_L to evaluate settlement lies our inability to predict which mechanisms prevail. The aim of this paper is to examine how changes in the ratio of B/D_L affect the produced deformation mechanisms. For this purpose, three centrifuge tests are presented, each corresponding to a different value of B/D_L. For each test, the produced deformation mechanisms are identified through displacement vector fields corresponding to the liquefiable layer.

Experimental Methods

The three centrifuge experiments (OA4, OA6, and OA8) discussed in this paper represent plane strain problems. A strip foundation applying a bearing pressure of 50 kPa is considered, resting on a liquefiable layer of loose sand, whose thickness changes for each test. The width of the foundation is 4.65 m in prototype scale. The liquefiable layers rest on a rigid base. More details are given in Table 1 and schematic cross-sections can be found in Figure 1. Aspect ratios are calculated by dividing the height of the structure's centre of mass with the width of its foundation.

Table 1. Important parameters of centrifuge tests (in prototype scale).

Test	**Depth of liquefiable layer, D_L (m)**	**Bearing pressure, q (kPa)**	**Relative density, Dr (%)**	**Width of foundation over depth of layer, B/D_L**	**Aspect ratio, H/B**
OA4	11.5	50	39	0.4	0.58
OA6	4.6	50	42	1.0	0.58
OA8	2.3	50	40	2.0	0.58

All experiments were performed on the Turner Beam Centrifuge, at the Schofield Centre of the University of Cambridge. The layers were prepared by air pluviation of Hostun sand, using an automatic sand pourer (Madabhushi et al., 2006). The instrumentation used consisted of miniature piezoelectric accelerometers, micro electro-mechanical systems accelerometers, pore pressure transducers, and linear variable displacement transducers. In order to overcome the

inconsistency between the scaling laws of dynamic and seepage time in centrifuge modelling (Madabhushi, 2014), a high viscosity aqueous solution of hydroxypropyl methylcellulose was used for the saturation of the sand layers. The centrifugal acceleration applied was 50 g, so the pore fluid had a viscosity of 50 cSt. The model container was a rigid box. One of its sides contained a Perspex window, through which a high frame-rate camera could capture the seismic response. PIV analysis (White et al., 2003) was performed on the recorded images, in order to obtain deformation vector fields. Layers of Duxseal limited the effect of the rigid boundaries (Steedman and Madabhushi, 1991). A stored angular momentum actuator (Madabhushi, 1998) was used to generate sinusoidal pseudo-harmonic input motions. The excitations were of 0.2 g peak acceleration, 20 s duration, and 1 Hz frequency for all tests (values in prototype scale).

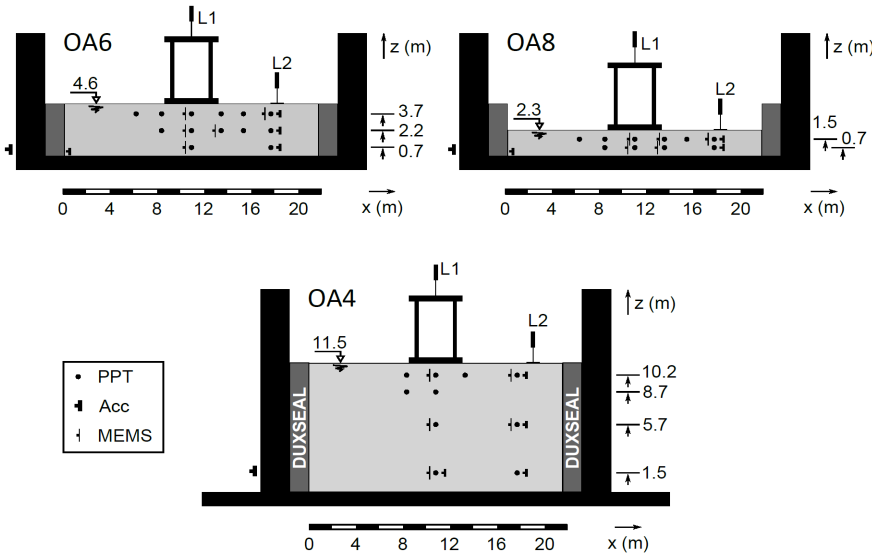

Figure 1. Models tested. Dimensions are in meters (prototype scale). Pore Pressure Transducers (PPTs), Piezoelectric accelerometers (Acc), and Micro Electro-Mechanical Systems accelerometers (MEMS) were used in the soil. L1 and L2 are displacement transducers.

Results and Discussion

The deformation mechanisms developed during the experiments are shown in Figure 2. Figure 2a depicts the displacements corresponding to the whole duration of the seismic motion, whereas Figure 2b only focuses on one half of the fifth cycle of soil response. All displacements are calculated relative to the rigid base. Displacements generated during post-earthquake reconsolidation are not included in these plots since in all cases their contribution to the settlement of the structure was limited. The zero of the ordinate in these graphs signifies the base of the layer. In the case of test OA4, the area that could be captured by the camera is a portion of the whole cross-section. Horizontal and vertical displacement contours corresponding to Figure 2a are presented in Figure 3. Each test will be analysed below. Firstly, the displacement mechanism will be discussed and then the movements of the soil surface will be pointed out, as they could be important for utilities or for estimating the behaviour of neighbouring structures.

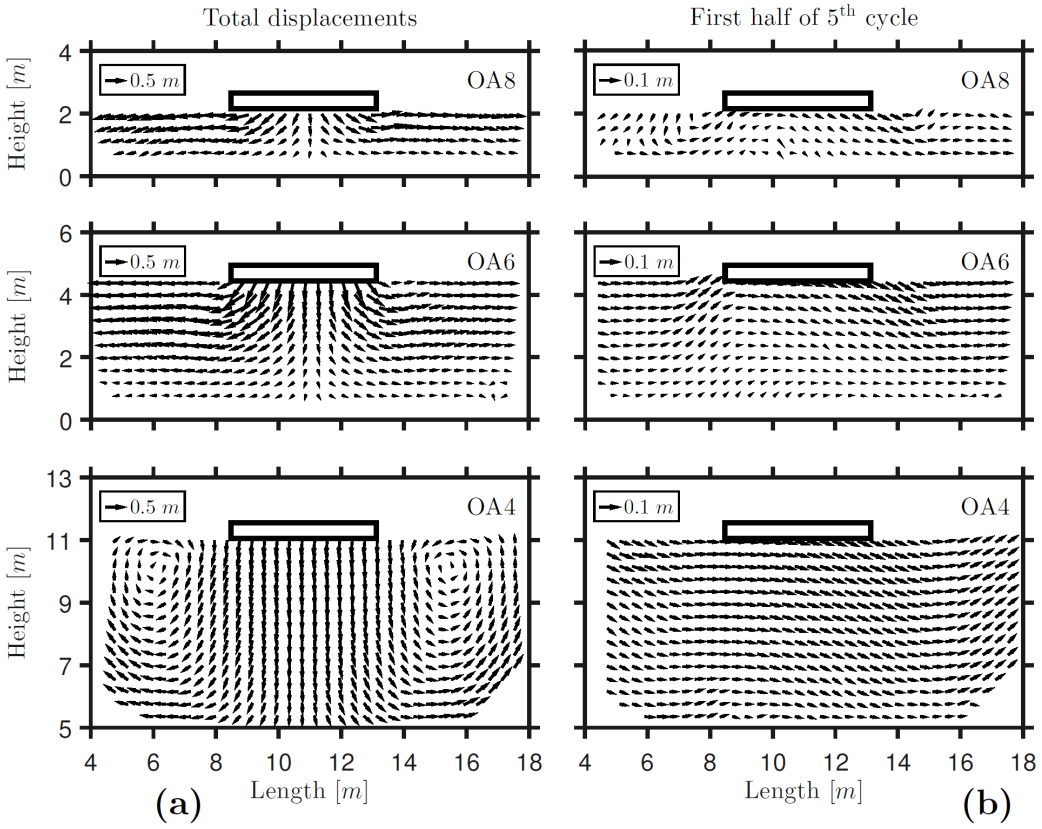

Figure 2. Displacement vectors, calculated relative to the rigid base. Vector length scale is 1. (a) whole duration of the seismic motion, (b) first half of the fifth cycle of the motion.

Test OA4 (B/D_L=0.4)

The displacement vectors of Figure 2a reveal an extended mechanism. The area monitored by the camera, 3B in length and 1.3B in depth, does not engulf all displacements. The soil under the footing moves almost exclusively vertically, as can be seen in Figure 3. The surrounding soil is pushed outwards. At a distance of about 0.6B from the edges of the foundation and at a depth of about 0.25B from the surface, points of rotation can be observed, around which the liquefied soil revolves, in what resembles the mobilisation of a bearing capacity failure mechanism.

Figure 2b pictures a half-cycle and reveals the mechanism more clearly. As already mentioned, the displacements are calculated relative to the rigid base. During this half cycle, the base moves to the left. Due to inertia, the soil layer appears to move to the right, while the structure rotates clockwise. The area underneath the foundation retains increased effective stresses throughout the seismic motion, due to the bearing pressure of the structure as well as due to static shear. However, it moves significantly relative to the rigid base because the fully liquefied soil of the free-field cannot offer it any lateral support. The result is the mobilisation of an extended failure mechanism that reaches a depth of more than 1B. The liquefied soil to the right of the foundation is easily pushed outwards, forming a passive zone and allowing the structure to settle. The upwards movement of this zone is facilitated by the proximity of the boundary, situated at about

8 m from the edge of the structure (Figure 1). Underneath the left edge of the foundation, the soil does not settle, as it is unloaded and its excess pore pressures drop. Further to the left, an active wedge is formed. In the previous half-cycle, this zone would have moved upwards, just like the soil to the right of the foundation does during this half-cycle. Now, it is allowed to come back down as the zone of increased effective stress under the structure moves to the right. Overall, the settlement of the structure is predominantly driven by the mobilisation of an extended failure mechanism, where a mass of soil underneath the foundation accumulates vertical displacement with each half-cycle, as it loses lateral support from the surrounding soil. Along with this mechanism, localised volumetric strains due to drainage add to displacements.

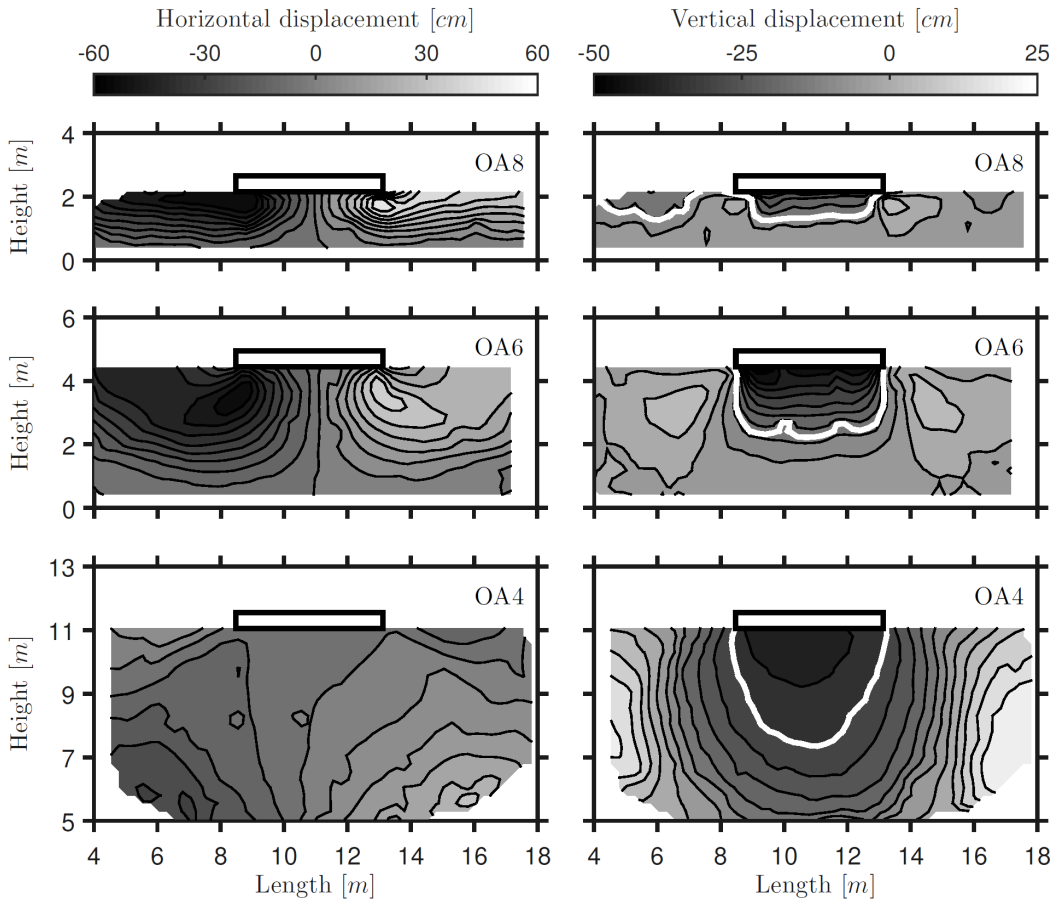

Figure 3. Horizontal and vertical displacement contours, for the whole duration of the seismic motion. The highlighted vertical contour corresponds to the settlement of the free-field.

According to the method of Tokimatsu and Seed (1987), the expected value of free-field settlement for this test is 30 cm. This value corresponds to the highlighted vertical contour in Figure 3. Only the foundation settles more, with the soil surface next to it and up to a distance of 0.6B settling less, whereas further away the surface is pushed upwards. It should be noted that due to the extent of the mechanism, it is possible that the upwards movement of soil towards the edges of the box is facilitated by the boundaries. The maximum upward displacement is observed at about 1B from the edges of the foundation. LVDT L2 (Figure 1), placed at that

distance, reaches up to 10 cm of upward displacement. The maximum settlement of the foundation relative to the soil right next to it is 15 cm. After the seismic motion is over, the soil layer reconsolidates. A few minutes after the earthquake, the soil surface rests and a heave is visible next to the structure. Its peak, 30cm higher than the free-field, is located at about 1B from the edges of the structure.

Test OA6 ($B/D_L=1$)

In test OA6, the displacement mechanism is more localised (Figure 2a). Here, it is also soil from under the edges of the footing that is displaced laterally. In fact, the largest horizontal movements are observed under the edges of the foundation (Figure 3). Large settlements only occur under the structure.

Figure 2b depicts a half-cycle of ground displacement. A soil column of increased effective stress forms between the foundation and the rigid base, allowing for a more violent structural response. As the structure rotates clockwise, the soil under its right edge is required to withstand increased shearing while becoming weaker, as pore pressures rise due to localised compression. Inevitably, it is laterally displaced outwards, pushing along the fully liquefied soil of the free-field, which is unable to provide significant resistance. Localised drainage of the rising pore pressures is a potential cause for the increased settlement observed to the right of the foundation. The left edge of the footing moves upwards, unloading the area underneath it, which does not settle, and reducing pore pressures. As the soil of the free-field moves towards the structure, it encounters a zone of increased effective stress that it cannot push and is hence forced to divert upwards. Through the course of the earthquake, settlement and horizontal displacements accumulate (Figure 2a, Figure 3). Overall, cumulative settlement is the result of a mechanism during which soil from underneath the structure is pushed outwards with each half-cycle of movement. In this case, the cyclic shearing imposed by the foundation dominates in driving localised soil displacements. Localised drainage is also of importance.

LVDT L2 (Figure 1) captures 12 cm of free-field settlement, a value identical to that predicted by the method of Tokimatsu and Seed (1987) for this layer. In figure 3, this value of settlement corresponds to the highlighted vertical contour. Greater settlement is only observed for the structure itself, with the soil surface up to a distance of about 1B from the edges of the foundation settling less than the free-field. A few minutes after the earthquake, reconsolidation is over and a small heave is observed right next to the structure and up to a distance of about 1B from its edges, with the peak being about 10 cm higher than the free-field. The relative settlement between the structure and the soil right next to it is about 45cm. Significant horizontal displacements are also observed. These displacements are as large as 25cm at the surface and can extend up to 2B from the edges of the foundation (Figure 3).

Test OA8 ($B/D_L=2$)

The thinnest layer examined is that of test OA8. Despite what would be anticipated, either by free-field methods (e.g. Tokimatsu and Seed, 1987) or by empirical charts (Liu and Dobry, 1997), the structure settles significantly. LVDT L1 (Figure 1) captures 33cm of co-seismic settlement for the structure. The overall displacement mechanism depicted in Figure 2a shows that settlement can be mainly attributed to soil being displaced from underneath the foundation.

In Figure 2b, a half-cycle is depicted. The area under the foundation, where full liquefaction is not reached, follows the movement of the rigid base more closely than the fully liquefied soil of the free-field. As the structure rotates clockwise, it imposes significant compression to the soil under its right edge, forcing a surge in pore pressures. The weakened soil is displaced outwards as no significant lateral support can be provided from the liquefied soil of the free field. Settlement accumulates as more soil is displaced with each half-cycle. Localised drainage also contributes to the generation of settlements. Under the left edge of the foundation, pore pressures drop as the structure rotates clockwise, locally increasing effective stresses. As in OA6, the soil to the left of the structure encounters this zone of increased effective stress and moves upwards, following the rotation of the foundation. On the whole, it is soil-structure interaction imposed cyclic loading that mainly drives displacements. As in OA6, localised drainage is of importance.

The settlement captured by LVDT L2 (Figure 1) is 9 cm, close to the 7 cm that the method of Tokimatsu and Seed (1987) predicts for the free-field. The highlighted vertical contour of Figure 3 corresponds to 9 cm. Settlements larger than those of the free-field are observed underneath the foundation and also to its left, up to a distance of 1B from its edge. These increased settlements next to the foundation are due to the existence of the structure, which during the earthquake accumulates counter-clockwise rotation. This rotation leads to higher excess pore pressures under the left edge of the foundation. As these pressures dissipate, they keep the area next to the structure liquefied for a longer duration and cause an increase in settlement. To the right of the foundation, vertical displacements are similar to those of OA6, albeit more localised. A small heave forms at the surface, but it does not extend further than 0.5B from the edge of the foundation. The settlement of the structure relative to the soil next to it is 25 cm. The horizontal contours of Figure 3 reveal large horizontal movements of as much as 50cm at the surface next to the structure.

Conclusions

The focus of this paper is on the deformation mechanisms that develop under a shallow footing resting upon a liquefiable layer, in the event of an earthquake. Three centrifuge tests are presented, each corresponding to a different value of B/D_L, where B is the width of the structure and D_L is the depth of the liquefiable layer. In test OA4, where $B/D_L=0.4$, an extended failure mechanism is mobilised. The structure settles as the soil underneath it loses lateral support from the fully liquefied soil of the free-field. In test OA6, where $B/D_L=1$, the settlement of the structure is primarily caused by soil-structure interaction imposed cyclic loading, gradually pushing out soil from underneath the foundation. During test OA8, where $B/D_L=2$, an exacerbated version of the mechanism of test OA6 is observed, with displacements being even more localised. Transient hydraulic gradients and localised drainage are of importance for all three tests.

Considering the results presented here, it is evident that volumetric mechanisms affecting the whole layer are not prevalent for any case. Consequently, methodologies that rely on such mechanisms are not appropriate. For small values of B/D_L parameters relevant to bearing capacity failure should be considered, whereas for values of B/D_L above 1 the focus should be on localised soil-structure interaction.

The parameter examined in this paper was the ratio of B/D_L, hence all other parameters were kept unchanged. Further research should focus on the relative density of the sand, the type of the seismic motion, the aspect ratio and the bearing pressure of the structure.

Acknowledgments

The centrifuge tests were carried out with the excellent assistance of the technicians of the Schofield Centre, who are hereby acknowledged. Moreover, the first author would like to thank Qualcomm, the Vergottis family and the Foundation for Education and European Culture for their financial support.

References

Bertalot D, Villalobos FA, Brennan, AJ (2013) Influence of bearing pressure on liquefaction-induced settlement of shallow foundations, Géotechnique, ***63****(5): 391-399*

Bray J, Sancio R, Durgunoglu T, Onalp A, Youd T, Stewart J, Seed R, Cetin O, Bol E, Baturay M, Christensen C, Karadayilar T (2004) Subsurface Characterization at Ground Failure Sites in Adapazari, Turkey, Journal of Geotechnical and Geoenvironmental Engineering,130(7): 673-685

Cubrinovski M, Bradley B, Wotherspoon L, Green RA, Bray JD, Wood C, Pender M, Allen J, Bradshaw A, Rix G, Taylor M, Robinson K, Henderson D, Giorgini S, Ma K, Winkely A, Zupan J, O'Rourke T, DePascale G, Wells D (2011) Geotechnical Aspects of the 22 February 2011 Christchurch Earthquake, Bulletin of the New Zealand Society for Earthquake Engineering, 44(4): 205-226

Dashti S, Bray JD, Pestana JM, Riemer M, Wilson D (2010) Mechanisms of Seismically Induced Settlement of Buildings with Shallow Foundations on Liquefiable Soil, Journal of Geotechnical and Geoenvironmental Engineering, 136(1): 151-164

Liu L and Dobry R (1997) Seismic Response of Shallow Foundation on Liquefiable Sand, Journal of Geotechnical and Geoenvironmental Engineering, 123(6): 557-567

Madabhushi SPG (2014) *Centrifuge Modelling for Civil Engineers*, Taylor & Francis, Boca Raton, Florida, USA

Madabhushi SPG, Houghton NE, Haigh SK (2006) A new automatic sand pourer for model preparation at University of Cambridge, Proceedings of the Sixth International Conference on Physical Modelling in Geotechnics, Hong Kong, 4-6 August, 217-222

Madabhushi SPG, Schofield AN, Lesley S (1998) A new Stored Angular Momentum (SAM) based Earthquake Actuator, Proceedings of the International Conference on Geotechnical Centrifuge, Tokyo, Japan, 23-25 September

Steedman RS and Madabushi SPG (1991) Wave propagation in sand medium, Proceedings of the 4th International Conference on Seismic Zonation, Stanford, California, 26-29 August

Tokimatsu K and Seed HB (1987) Evaluation of Settlements in Sands Due to Earthquake Shaking, Journal of Geotechnical Engineering, 113(8): 861-878

White DJ, Take WA, Bolton MD (2003) Soil deformation measurement using particle image velocimetry (PIV) and photogrammetry, Géotechnique, 53(7): 619-631

Yasuda S, Harada K, Ishikawa K, Kanemaru Y (2012) Characteristics of liquefaction in Tokyo Bay area by the 2011 Great East Japan Earthquake, Soils and Foundations, 52(5): 793-810

Yoshimi Y and Tokimatsu K (1977) Settlement of buildings on saturated sand during earthquakes, Soils and Foundations, 17(1): 23-38